

Star formation and chemical evolution in SPH simulations: a statistical approach

Cesario Lia^{1,2}, Laura Portinari^{3,2}, and Giovanni Carraro²

¹ *SISSA/ISAS, via Beirut 4, I-34014 Trieste, Italy*

² *Dipartimento di Astronomia, Università di Padova, Vicolo dell'Osservatorio 2, I-35122 Padova, Italy*

³ *Theoretical Astrophysics Center, Juliane Maries Vej 30, DK-2100 Copenhagen Ø*

E-mail: lportina@tac.dk, carraro@pd.astro.it

Submitted: March 2001; accepted: November 2001

ABSTRACT

In Smoothed Particles Hydrodynamics (SPH) codes with a large number of particles, star formation as well as gas and metal restitution from dying stars can be treated statistically. This approach allows to include detailed chemical evolution and gas re-ejection with minor computational effort. Here we report on a new statistical algorithm for star formation and chemical evolution, especially conceived for SPH simulations with large numbers of particles, and for parallel SPH codes.

For the sake of illustration, we present also two astrophysical simulations obtained with this algorithm, implemented into the Tree-SPH code by Lia & Carraro (2000). In the first one, we follow the formation of an individual disc-like galaxy, predict the final structure and metallicity evolution, and test resolution effects.

In the second one we simulate the formation and evolution of a cluster of galaxies, to demonstrate the capabilities of the algorithm in investigating the chemo-dynamical evolution of galaxies and of the intergalactic medium in a cosmological context.

Key words: hydrodynamics - methods:numerical - stars: formation - galaxies: evolution - galaxies: chemical evolution

1 INTRODUCTION

The evolution of chemical abundances in the Universe is nowadays a subject of utmost importance. Relevant issues are when and where the first metals were synthesized, and how they spread to enrich the individual host galaxies, as well as the intergalactic (IGM) and intracluster (ICM) medium; see Ferrara et al. (2000) and Chiosi (2000) for recent papers on the subject.

To assess these issues, related to metal production and mixing into the interstellar medium (ISM), it is necessary to couple chemical evolution with hydrodynamical evolution. This has been done several times in the past, with different techniques. Although in this paper we specifically deal with chemical evolution in Smoothed Particle Hydrodynamics (SPH), we like to recall also some works based on eulerian codes for the hydrodynamics. The production and distribution of metals over cosmic scales has been recently addressed by Cen & Ostriker (1999) and by Yepes et al. (1998), who implemented elementary prescriptions for metal enrichment in their cosmological simulations. Chemo-dynamical models for individual galaxies, considering a multi-phase ISM have been developed by Burkert & Hensler (1988), Burkert et al. (1992), Theis et al. (1992), Samland et al. (1997).

More recently, Recchi et al. (2001) implemented the detailed production and mixing of many different chemical elements in their hydro-code for dwarf starburst galaxies.

The first attempt to couple SPH with chemical evolution is by Steinmetz & Müller (1994), who study the formation of a Milky Way-like galaxy in a cosmological context. Their chemical evolution scheme is rather simple: they consider the ejection of gas and global metallicity Z from Type II supernovæ (SN II), occurring over 30 Myr after the star formation (SF) episode. These gas and metals produced by a star particle are then distributed around over the neighbouring gas particles.

More detailed schemes have been worked out by Raiteri et al. (1996) and Berczik (1999). Raiteri et al. model the evolution of oxygen and iron, making use of fitting formulae to follow gas and metal ejection from a star particle over time. Moreover, they include the delayed iron production by Type Ia SN (SN Ia), by implementing the theoretical rate by Greggio & Renzini (1983, hereinafter GR83). The gas and metals produced by a star particle are distributed around over the neighbouring gas particles, as in Steinmetz & Müller (1994). Berczik follows the method developed by Raiteri et al., adding planetary nebulae, hydrogen and helium to the picture. From the chemical point of view, the

main improvement of these models is that they avoid the Instantaneous Recycling Approximation (IRA, e.g. Tinsley 1980) by taking into account the different stellar sources and production timescales of the various elements.

Carraro et al. (1998) and Buonomo et al. (2000) consider the evolution of the overall metallicity in the IRA, with a scheme similar to Steinmetz & Müller (1994). However, in the feedback computation they also include the effect of SN Ia according to the rate by GR83, and they introduce a metal diffusion mechanism instead of the standard SPH smoothing of metallicity among gas particles.

Recently, Mosconi et al. (2001) presented a new implementation of chemical evolution in SPH, following the evolution of very many elements. They consider metal production from SN II, essentially instantaneous, and the contribution of SN Ia. The latter, rather than following the theoretical rate and time distribution by GR83, is treated simply as a prompt metal release occurring after a given time-delay t_{SNI} after the SF episode. The typical time-delay t_{SNI} , as well as the number of SN Ia with respect to SN II, are introduced as free parameters in their simulations.

All the above mentioned models display one or both of the following numerical drawbacks:

(i) New collisionless star particles are created when SF occurs, while the corresponding metal ejecta are redistributed around to other gas particles. Hence, the number of SF episodes and of “offspring stars” per gas particle must be artificially damped, otherwise the overall number of particles gets too large. Also, the simulation must start with relatively few baryonic particles, as SF will increase their number substantially in the course of the simulation; this hampers the modelling of the early, very interesting phases of galaxy formation.

(ii) When SF occurs, hybrid particles are created which host both gas and different stellar populations. As hybrid particles consist of both collisional and collisionless sub-components, from the point of view of the hydrodynamics they introduce artifacts: before becoming purely collisionless particles, the stars tend to follow for a while the dynamical evolution of the gas, clearly a spurious effect.

In this paper, we present a new statistical algorithm of SF and chemical evolution in the context of N-body SPH simulations, aimed at overcoming the above mentioned problems. In our approach, in fact, the number of baryonic particles remains constant throughout the simulation, and particles are either fully hydrodynamical or fully collisionless.

Due to its low computational costs, the new formalism is particularly suited to many-particle simulations, and the completely local character of the computation of “chemical quantities” makes it convenient for parallel codes (Lia 2000, Lia & Carraro 2000, Dalla Vecchia 2001, Lia et al. 2001).

The scheme follows the detailed production of many chemical elements over different timescales, avoiding the IRA. In this respect, we provide updated fitting formulae for the evolution of gas and metal release, that can be easily implemented also in other particle-based codes. The approach allows to calculate the abundance evolution of a number of chemical elements independently, as well as of the global metallicity. Depending on the objects being modelled, one might in fact be interested in monitoring different chemical elements in different cases.

We remark that relaxing the IRA is fundamental not

only for the sake of chemical evolution (to trace abundance ratios of different elements, for instance $[\alpha/\text{Fe}]$ ratios), but also for the effects that delayed gas restitution may have on the dynamics, as recently discussed by Jungwiert et al. (2001). Among others, continuous mass loss from stars over a Hubble time contributes to solve Robert’s time paradox in spiral galaxies (Kennicutt et al. 1994).

The layout of the paper is as follows. In Section 2 we briefly introduce our TreeSPH code, while in Section 3 we describe the star formation algorithm and related feedback prescriptions. Section 4 provides a detailed explanation of our statistical chemical model, whereas Sections 5 to 8 present tests and astrophysical applications. Finally, Section 9 summarizes our findings.

2 THE N-BODY TREE-SPH CODE

The simulations presented here have been performed using the Tree-SPH code developed in Carraro et al. (1998), Lia (2000), Lia & Carraro (2000) and Dalla Vecchia (2001). In this code, the properties of the gaseous component are described by means of the SPH technique (Lucy 1977; Gingold & Monaghan 1977), whereas the gravitational forces are computed by means of the hierarchical tree algorithm of Barnes & Hut (1986), using the tolerance parameter $\theta = 0.8$, expanding the tree nodes to quadrupole order, and adopting a spline softening parameter. In the SPH method, each particle represents a fluid element whose position, velocity, energy, density etc. are followed in time and space. The properties of the fluid are locally estimated by an interpolation which involves the smoothing length h . Convergence tests for the SPH part of the code were performed in Carraro et al. (1998). Finally, cooling tables as a function of the metallicity of the gas have been taken from Sutherland & Dopita (1993). For further details, we refer the reader to the above mentioned papers.

In this paper we improve upon the SF and Chemical Evolution sections of our code, as presented here below.

3 STAR FORMATION AND FEED-BACK

The formation of stars is a poorly understood process, and therefore difficult to model properly. The most widely used strategy consists of two steps.

Firstly, an element of fluid must satisfy some conditions to be eligible to SF. The basic criteria adopted in our SPH code to select the fluid elements prone to SF are (i) the gas particle must be in a convergent flow, and (ii) the gas particle must be Jeans unstable. The conditions are met if the velocity divergence is negative and if the sound crossing time-scale is shorter than the dynamical time-scale. The effect of varying the SF criteria has been discussed in details in Buonomo et al. (2000), which the reader is referred to.

Secondly, the fluid element turns into stars according to a suitable star formation rate (SFR), which is customarily a reminiscence of the Schmidt (1959) law:

$$\frac{d\rho_\star}{dt} = -\frac{d\rho_g}{dt} = c_\star \frac{\rho_g}{t_{ff}}$$

where c_\star is the star efficiency parameter, that we set equal

to 0.1, and t_{ff} is the free-fall timescale. In our code, this SF law is seen as the probability that a single gas particle is completely transformed into a star particle in the next time step (Katz & Gunn 1991; Katz et al. 1996). This probability is computed as

$$P(SF) = 1 - \exp\left(-\frac{c_* \Delta t}{t_{ff}}\right) \quad (1)$$

where Δt is the particle time step. The particle is then effectively chosen, or not, to transform into a star particle by means of a Monte Carlo method. This statistical approach is the more reliable the larger is the number of particles that model the star forming region.

The advantage of this approach is twofold. First of all, the total number of particles in the simulation does not increase, since a gas particle turns completely into a star particle once it fulfills all the SF criteria. Besides, baryonic particles are assigned and always retain all the same mass throughout the simulation. Secondly, at increasing number of particles enclosed in a star forming region, the probability approach naturally becomes more and more realistic. Again, this makes it potentially advantageous for algorithms running on parallel computers, where large numbers of particles can be managed (Lia 2000; Dalla Vecchia 2001).

Stars are expected to return energy to the ISM via SN explosions, and the bulk of the energy released in the ISM is known as the stellar energy Feed-Back. In our code, the SN rates are calculated by the statistical algorithm as explained later in this paper, and each SN is assumed to contribute 10^{50} erg of energy to the surrounding medium (Thornton et al 1998).

The key problem here is to know how the released energy is given to the ISM, because the limited resolution of N-body simulations does not allow to describe the ISM as a multi-phase medium. In Buonomo et al. (2000) we have investigated different prescriptions for the Energy Feed-Back, suggesting that a good solution is to release all the energy from SN and other sources to the thermal budget of the fluid element (Steinmetz & Müller 1994). As in this scheme the feed-back is localized within the gas particle, and gets rapidly dissipated by cooling, it turns out to have no significant effects on the dynamics and/or on the chemical properties of the gas through the mixing of metals (which is treated independently, see § 4.4).

4 THE “STATISTICAL” CHEMICAL ALGORITHM

Once stars are present, they return to the ISM part of their mass, in form of chemically processed gas, and energy, via the stellar feed-back. In this paper we extend the probabilistic approach adopted for the SF process to the energy and chemical feed-back. Each baryonic particle can be either in the form of gas or in the form of stars. The probability that a particle turns from gas to stars is fixed by the SFR (Eq. 1). Likewise, each star particle can be assigned a certain probability to turn back into gas; and when this takes place, the particle carries along the corresponding metal production, SN rate, and energy feed-back. Notice that in the present approach all baryonic particles, stars and gas, have the same

mass and their total number is conserved. Our statistical algorithm is developed and only valid under this condition.

In brief, we consider a star particle as a Single Stellar Population (SSP) of assigned Initial Mass Function (IMF), and calculate the fraction of its mass which turns into re-ejected gas, as a function of its age. This mass fraction is identified as the probability that a star particle of age t becomes a gas particle again at time $t + \Delta t$, being Δt the particle time step. For a Salpeter IMF, for instance, this probability is of the order of 30% over a Hubble time, since this is the fraction of the initial mass of the SSP which is globally re-ejected. By means of a Monte Carlo method, at each timestep we transform back into gas a certain fraction of the star particles; typically a 30% of the total stars formed will have become gas again by the end of the simulation, after a Hubble time. Over a large enough number of particles, star formation and the corresponding gas restitution should be well represented statistically. Besides, this approach easily takes into account that gas restitution from stars is diluted in time, with no need to assume the IRA.

Our statistical chemical algorithm is described in detail in the following sections.

4.1 Gas restitution

Each star particle is treated as a SSP of total mass m and age $t = T - T_0$, where T is the present age of the system and T_0 is the birth-time of the star particle. Ideally, one could follow the detailed chemical, photometric and spectral evolution of each SSP by adopting a grid of stellar models (e.g. Chiosi et al. 1998). However, in a hydrodynamical code this would heavily increase the computational load. To circumvent this, we prefer to approximate the amount of released gas, the SN rates and the metal production by means of analytical formulas, as described here below.

Within a SSP, stellar masses are distributed according to the IMF $\Phi(M)$, usually a power-law (e.g. $\Phi(M) \propto M^{-1.35}$ for a Salpeter IMF). A star of given mass M is characterized by a lifetime $\tau(M)$; when it “dies”, part of it remains enclosed in a remnant of mass M_r (a white dwarf, a neutron star or a black hole) while the rest is ejected back to the ISM in the form of chemically processed gas. Stellar models provide τ and M_r as a function of M . The mass fraction of the SSP which is ejected back in the form of gas by time $T = T_0 + t$ is:

$$E(t) = \int_{M(t)}^{M_u} \frac{M - M_r(M)}{M} \Phi(M) dM = \int_{\tau(M_u)}^t e(t') dt'$$

where

$$e(t) = \left[\frac{M - M_r(M)}{M} \Phi(M) \left(-\frac{dM}{d\tau} \right) \right]_{M(t)} \quad (2)$$

$M_u = 100 M_\odot$ is the upper stellar mass limit in the IMF, $M(\tau)$ indicates the mass of a star with lifetime τ , and $M(t) = M(T - T_0)$ is thus the smallest stellar mass dying and restituting gas by time T (see also Tinsely 1980). For a Salpeter IMF, for instance, the global returned gas fraction E over a Hubble time is of the order of 30%.

Accordingly, $e(t)$ of Eq. (2) is the rate of gas ejection in time. In our statistical approach, this rate is interpreted as the *probability* that a star particle, in time, transforms again

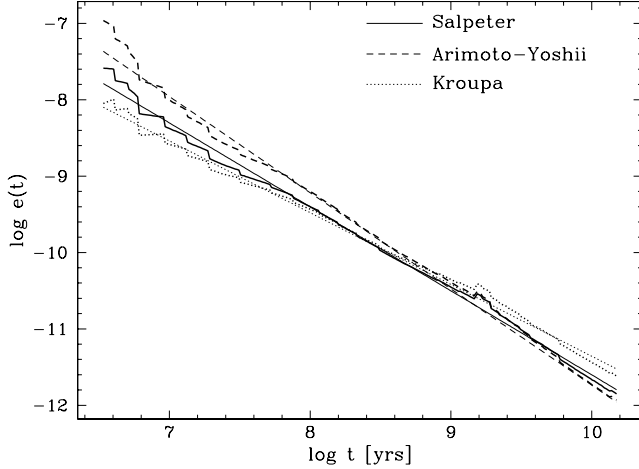


Figure 1. Rate of gas restitution for SSPs with different IMFs, as a function of the age t of the SSP. *Thick lines:* numerical results; *thin lines:* corresponding power-law fits. The function $e(t)$ represents as well the probability per year that a star particle transforms back into a gas particle (see text).

into gas. Namely, at each time step Δt the star particle is assigned a probability

$$g_t(\Delta t) = \int_t^{t+\Delta t} e(t') dt' \quad (3)$$

to turn back into gas, and a Monte Carlo method decides whether it does switch to a gas particle within Δt . The overall probability that a star particle ever switches to gas again, integrated over time, is $E \sim 30\%$; accordingly, of all the star particles formed at time T_0 roughly one third will have returned to be gas after a Hubble time. Over a sufficiently large number of particles, this approach should give a fair representation not only of the overall gas restitution, but also of its rate in time (avoiding the IRA).

Actually if, say, N particles become star particles at some time T_0 , to yield the correct gas restitution in time the probability (3) should be applied to all of those N particles, at each timestep, throughout the simulation. However, by age t a fraction $E(t)$ of those N particles will have already returned to be gas, while only a fraction $1 - E(t)$ will still be stars. Obviously, the probability to transform back into gas at age t can be calculated only for those $N [1 - E(t)]$ particles that are still stars at that time, rather than on the base of the whole initial population of N particles. Hence, to recover the correct statistical gas restitution, the probability (3) must be corrected by a further factor $[1 - E(t)]$, and becomes:

$$g_t(\Delta t) = \frac{\int_t^{t+\Delta t} e(t') dt'}{1 - E(t)} \quad (4)$$

Our test in § 5 and Fig. 4 demonstrate that in this way the correct global gas restitution is statistically recovered — which would not be the case if expression (3) for the probability were directly used.

We should now determine $e(t)$ as a function of the age t of the SSP. As mentioned above, in terms of computational effort it is convenient to adopt some analytical fit to the numerical results of detailed chemical evolution models. We proceed as follows.

Salpeter	Kroupa	Arimoto–Yoshii
$e(t) = 0.25 t^{-1.1}$	$e(t) = 0.011 t^{-0.94}$	$e(t) = 7.3 t^{-1.26}$
$t[yr] > \tau(M_u) = 3.4 \cdot 10^6$		

Table 1. Rate of gas restitution $e(t)$ for SSPs with different IMFs; $e(t) = 0$ for $t < 3.4$ Myr, lifetime of the most massive star, $M_u = 100 M_\odot$. $e(t)$ represents as well the probability per year that a star particle transforms back into a gas particle (see text).

We calculate numerically the function (2) adopting the stellar lifetimes $\tau(M)$ and remnant masses $M_r(M)$ from the Padova evolutionary tracks (see Portinari et al. 1998, hereinafter PCB98, and references therein). Regarding the IMF, its shape and variations with the environment are still an open issue (e.g. Scalo 1998); hence we consider three different IMFs suggested in literature, with the intent of covering a representative range of possibilities.

- (i) The standard and widely adopted Salpeter (1955) IMF

$$\Phi(M) = C_s M^{-1.35} \quad C_s = 0.1716$$

- (ii) The somewhat steeper IMF by Kroupa (1998), best suited to the Solar Neighbourhood:

$$\Phi(M) = \begin{cases} C_{k1} M^{-0.5} & M < 0.5 \\ C_k M^{-1.2} & 0.5 < M < 1 \\ C_k M^{-1.7} & M > 1 \end{cases}$$

$$C_{k1} = 0.48 \quad C_k = 0.295$$

- (iii) The more top-heavy IMF suggested by Arimoto & Yoshii (1987) for elliptical galaxies:

$$\Phi(M) = C_a M^{-1} \quad C_a = 0.145$$

C_s , C_a , C_k and C_{k1} are normalization coefficients fixed so that the IMF is normalized to unit mass when integrated between the low and high stellar mass ends (0.1 and $100 M_\odot$ respectively). With the adopted stellar mass limits, SSPs with the Salpeter or Kroupa IMF reconstitute a 30% of their initial mass in gas, while for SSPs with the more top-heavy IMF by Arimoto & Yoshii the restitution fraction is larger (about 50%).

The numerical results for the function (2) are well fitted by power laws (Fig. 1); the fitting functions are listed in Table 1. In principle, stellar lifetimes and remnant masses depend also on the metallicity of the star (PCB98), and hence $e(t)$ also depends on the metallicity of the parent SSP. However, it is beyond the scope of this paper to implement chemical evolution in such fine detail; therefore, for gas restitution (and for the chemical yields below) we adopt fits independent of metallicity. Notice, however, that metallicity-dependent prescriptions can in principle be inserted in our approach, as a star particle always keeps track of the metallicity Z_0 of its host SSP (as we did for the sole case of the nitrogen yields in § 4.3.1).

With the analytical expressions given for $e(t)$ in Table 1, once the IMF is chosen it is straightforward to calculate, at each time step, the probability (4) that a star particle transforms back into gas. If this happens, in the following discussion we will call it a “gas-again particle”.

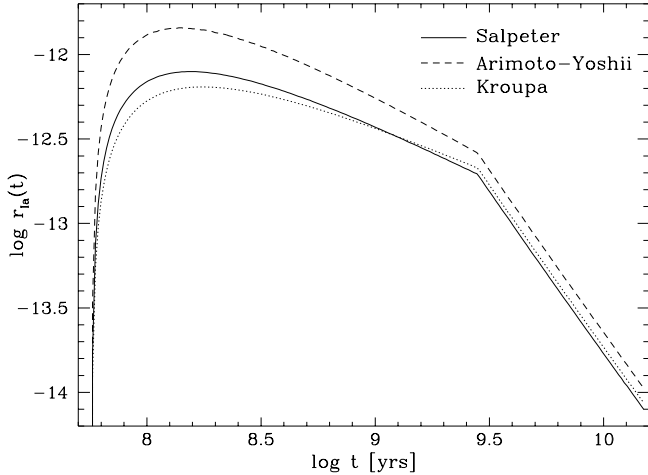


Figure 3. Rate of SN Ia for SSPs of age t and with different IMFs.

Accordingly, the rate of SN Ia in time is:

$$r_{Ia}(t) = \begin{cases} A \left[\left(-\frac{dM_2}{d\tau} \right) \int_{M_{B,min}}^{M_{B,max}} f\left(\frac{M_2}{M_B}\right) \frac{\Phi(M_B)}{M_B^2} dM_B \right]_{M_2(t)} & t \geq \tau(M_{up}) \\ 0 & \text{otherwise} \end{cases}$$

We calculate $r_{Ia}(t)$ numerically for our three IMFs and provide analytical fits to the numerical results (Fig. 3 and Table 2).

A particle of mass m which underwent SF produces in a time step Δt a number of SN Ia given by:

$$N_{SNIa} = m \int_t^{t+\Delta t} r_{Ia}(t') dt' \quad (6)$$

4.2.3 The statistical correction

So far, we have derived the SN rates for a SSP, and consequently for a particle which has experienced SF. When we are to calculate the feed-back effect that supernovae have on a given gas particle, in principle we need to know the number of SN produced in the time step Δt by all of its neighbouring particles which have experienced SF at some previous time. These include both star particles and gas-again particles. Although for each of these particles it is straightforward to calculate the corresponding N_{SNI} (5) and N_{SNIa} (6), the above mentioned procedure would require to determine all the neighbouring particles, both gas and stars. On the other hand, for hydrodynamical purposes only the neighbouring collisional (gas and gas-again) particles are of interest. So, in principle a double calculation of neighbours would be necessary, which would require a major computational effort and could not be trivially implemented in parallel codes.

We thus restrict the calculation of neighbours to gas particles, as usual in SPH codes. As a consequence, we can determine the contribution to the SN rate (and to the related feed-back, see Section 4) only from neighbouring gas-again particles; we should therefore correct for the “missing” contribution of star particles. We proceed as follows.

SN rates within the timestep Δt are calculated, rather than for all the particles that have experienced SF, only for those particles that return to be gas right *within* Δt . These particles represent a fraction $g_t(\Delta t)$ — given by (4) — of the whole parent stellar population. Accordingly, the “statistical correction” must be

$$N_{SN} \rightarrow \frac{N_{SN}}{g_t(\Delta t)} \quad (7)$$

Notice that in this approach not all gas-again particles (namely, any gas particles that have ever experienced SF in their past) contribute to the SN rates, but only those that become gas-again “right now”. This ensures that the SN explosions (and the metal production, see § 4.3.1 below) take place exactly where the parent stellar component is located.

The statistical correction (7) is quite large: a whole stellar population is sampled by the fraction of it which dies within the timestep Δt . This fraction can become very small, especially for small timesteps and/or at advanced ages after the SF episode (see the behaviour of $e(t)$ in time, Fig. 1). At late times, the hydrodynamical timestep of the system is very small with respect to the rate of gas restitution, hence statistical fluctuations in the number of old star particles turning to gas-again tend to become quite large. This might induce large fluctuations in the effective release of SN and metals with respect the smooth theoretical time evolution of a SSP. To hamper these fluctuation, the probability that a star particle becomes gas-again is computed, rather than over the dynamical timestep, over a “chemical timestep” which increases in proportion with the age of the SSP, so as to smoothen the related increase of the statistical noise. For the sake of clarity, from here on we indicate by Δt and δt the chemical and dynamical timestep respectively. The chemical timestep Δt is chosen to be the minimum between δt and one tenth of the age t of the SSP. We also put an upper limit to Δt of 2×10^8 yr, so that it does not become excessively large from the dynamical point of view, when we are dealing with stars that are a few Gyr old. 2×10^8 yr corresponds, for instance, to the typical revolution period of the Sun in the Galaxy.

In detail, our algorithm works as follows. For a star particle, the “Monte Carlo chance” to transform to gas-again is activated once every Δt , rather than at each dynamical step δt , with a corresponding probability (4) also calculated for Δt . If the star particle is selected to become a gas-again particle, it “produces” a number of SN (7) also calculated on the base of Δt . Before the next dynamical timestep, this particle is added to the list of gas particles for the calculation of neighbours, and from then on it behaves just like any other gas particle. Finally, it is worth noting that the energy feed-back is released over the hydrodynamical timestep, and the energy balance between cooling and heating is calculated over the hydrodynamical timestep, as well.

The various test applications presented later in this paper show that this statistical approach, with the adopted chemical timestep, yields sensible results.

4.3 Chemical enrichment

The calculation of the chemical enrichment of the gas proceeds in two steps:

- (i) calculation of metal production by SSPs in particles which have experienced SF;
- (ii) metal diffusion among gas particles.

In the tables we provide the necessary information to calculate the production of various chemical elements, as well as that of the overall metallicity, independently of one another. In fact, according to the particular object being modelled, one might be interested in tracking different chemical elements because available abundance data also depend on the class of object considered. Hence, in each simulation one can select and “switch on” the elements of interest. The hydrogen abundance, necessary to express chemical abundances in the usual [element/H] dex scale, can be obtained for each particle as:

$$X = 1 - Y - Z$$

where Y represent the helium mass fraction and Z the overall metallicity.

For the sake of clarity, here below we will describe our implementation of chemical evolution in terms of a single “metal parameter” Z . This parameter is meant to represent the chemical abundance of any specific chemical element — helium or metals.

4.3.1 Metal production of a star particle

Let’s consider a gas particle of metallicity Z_0 which becomes a star particle at time T_0 : it effectively hosts a SSP composed of a distribution of stellar masses $\Phi(M)$, all born at time T_0 out of gas with homogeneous metallicity Z_0 . As time progresses, stars of smaller and smaller mass M die, each ejecting a mass of metals given by:

$$M_Z = y_Z + Z_0(M - M_r)$$

The first term y_Z is the stellar yield, i.e. the newly synthesized metals (see the definition by Tinsley 1980 as revised by Maeder 1992); the second term is the metals present in the star from birth and re-ejected. The mass fraction that a SSP releases in the form of metals up to age t is:

$$\begin{aligned} E_Z(t) &= \int_{M(t)}^{M_u} \frac{M_Z}{M} \Phi(M) dM \\ &= \int_{M(t)}^{M_u} \frac{y_Z}{M} \Phi(M) dM + Z_0 \int_{M(t)}^{M_u} \frac{M - M_r}{M} \Phi(M) dM \\ &= \int_{\tau(M_u)}^t \left[y_Z \frac{\Phi(M)}{M} \left(-\frac{dM}{d\tau} \right) \right]_{M(t')} dt' + Z_0 E(t) \end{aligned}$$

Evidently, summing the E_Z ’s over all the chemical elements one expects:

$$\sum E_Z(t) = E(t)$$

The rate of metal ejection becomes:

$$e_Z(t) = p_Z(t) + Z_0 e(t)$$

which is determined once we know

$$p_Z(t) = \left[y_Z \frac{\Phi(M)}{M} \left(-\frac{dM}{d\tau} \right) \right]_{M(t)} \quad (8)$$

for the chemical element Z of interest, since $e(t)$ has already been calculated in § 4.1.

To calculate $p_Z(t)$, we adopt the stellar yields y_Z by PCB98 for the case of massive stars, and by Marigo (2001,

her case $\alpha = 1.68$) for low and intermediate mass stars. Similarly to what we did for the returned gas fraction and for the SN rates, we calculate the functions (8) numerically, for several chemical elements and for the three IMF cases. Then we provide suitable analytical fits to the numerical results, to be used in the hydrodynamical code. Our fitting functions are listed in Table 3. As in the case of the returned gas fraction, we neglect in general the dependence of stellar yields on the initial metallicity of the SSP.

The derived fitting functions reflect the different nucleosynthetic history of the various elements. Both helium and metals (meant as the overall metallicity) are expelled over the whole mass range; although the bulk comes from massive stars, the contribution from stars of intermediate and low mass cannot be neglected. Therefore, the “onset” of the fitting functions for He and Z corresponds to the lifetime of the most massive star (3.4 Myr) and the production continues forever; calculations have though been stopped at 15 Gyr, beyond that (which is beyond the age of the Universe anyways) the production can be considered negligible. The production rates rapidly decrease in time, due to the behaviour of stellar lifetimes with mass (cf. the factor $dM/d\tau$ in Eq. 8). The Arimoto–Yoshii IMF case is the most skewed toward massive stars, hence the metal production is the largest and it presents the steepest drop with time as it is the most dominated by massive stars. The global metal production is lower and its decrease with time is slower going to the Salpeter and then to the Kroupa IMF case.

Oxygen production, due to massive stars, is limited to the range of lifetimes of SN II progenitors (3.4 to 34 Myr). Especially for the most massive stars, oxygen production is sensitive to metallicity (PCB98). In the framework of a chemical algorithm handy enough to be implemented in hydrodynamical codes, it is not worth entering so much detail and we rather give average estimates of oxygen yields. Again, the global oxygen production is largest for the Arimoto–Yoshii IMF case and decreases going to the Salpeter and to the Kroupa case.

Similar trends, and comments, apply to the production of iron, magnesium, silicon, sulfur and calcium, also ejected by massive stars. Notice that we are discussing here only chemical yields from single stars; the contribution of SN Ia (binaries) will be added later. Theoretical magnesium yields are known to be underestimated with respect to observations (Timmes et al. 1995, Thomas et al. 1998, PCB98, Chiappini et al. 1999), while iron yields are sometimes suggested to be a bit high (though still within the intrinsic uncertainty of a factor of 2 in SN models, Timmes et al. 1995). The latter point is true especially when considering the latest estimates of the solar abundance $[Fe/H]_{\odot}=7.5$, rather than the old value of 7.67. In Table 3, entries for magnesium and iron have been optimized on the base of observational indications for the Solar Vicinity.

The nucleosynthetic history of carbon is quite composite. Carbon is ejected by massive stars through stellar winds and SN II explosions, while intermediate and low-mass stars contribute to its production in their TP-AGB phase. In both cases, theoretical carbon yields are sensitive to metallicity effects (PCB98, Marigo 2001). From the point of view of observations, the role of the various contributors and of metallicity dependence is still debated (Prantzos et al. 1994, Gustafsson et al. 1999, Gar-

chemical element		Salpeter	Kroupa	Arimoto–Yoshii	time range [yr]
Z	$p_Z(t) =$	$453\,t^{-1.7}$	$10.5\,t^{-1.5}$	$5919\,t^{-1.8}$	$t \in [3.4\,10^6, 15\,10^9]$
^4He	$p_{He}(t) =$	$2.8\,t^{-1.37}$	$0.14\,t^{-1.21}$	$80\,t^{-1.52}$	$t \in [3.4\,10^6, 15\,10^9]$
^{16}O	$p_O(t) = \left\{ \begin{array}{l} 7.3e-10 \\ 7.3e4\,t^{-2} \end{array} \right.$	$\begin{array}{l} 7.3e-10 \\ 7.3e4\,t^{-2} \end{array}$	$\begin{array}{l} 4.2e-10 \\ 4.2e4\,t^{-2} \end{array}$	$\begin{array}{l} 1.8e-9 \\ 1.8e5\,t^{-2} \end{array}$	$\begin{array}{l} t \in [3.4\,10^6, 10^7] \\ t \in [10^7, 3.4\,10^7] \end{array}$
^{56}Fe	$p_{Fe}(t) = \left\{ \begin{array}{l} 5.1e-11 \\ 5.1e3\,t^{-2} \end{array} \right.$	$\begin{array}{l} 5.1e-11 \\ 5.1e3\,t^{-2} \end{array}$	$\begin{array}{l} 3.3e-11 \\ 3.3e3\,t^{-2} \end{array}$	$\begin{array}{l} 1.1e-10 \\ 1.1e4\,t^{-2} \end{array}$	$\begin{array}{l} t \in [3.4\,10^6, 10^7] \\ t \in [10^7, 3.4\,10^7] \end{array}$
^{24}Mg	$p_{Mg}(t) = \left\{ \begin{array}{l} 4.6e-11 \\ 4.6e3\,t^{-2} \end{array} \right.$	$\begin{array}{l} 4.6e-11 \\ 4.6e3\,t^{-2} \end{array}$	$\begin{array}{l} 2.5e-11 \\ 2.5e3\,t^{-2} \end{array}$	$\begin{array}{l} 1.2e-10 \\ 1.2e4\,t^{-2} \end{array}$	$\begin{array}{l} t \in [3.4\,10^6, 10^7] \\ t \in [10^7, 3.4\,10^7] \end{array}$
^{28}Si	$p_{Si}(t) = \left\{ \begin{array}{l} 5.8e-11 \\ 5.8e3\,t^{-2} \end{array} \right.$	$\begin{array}{l} 5.8e-11 \\ 5.8e3\,t^{-2} \end{array}$	$\begin{array}{l} 3.6e-11 \\ 3.6e3\,t^{-2} \end{array}$	$\begin{array}{l} 1.3e-10 \\ 1.3e4\,t^{-2} \end{array}$	$\begin{array}{l} t \in [3.4\,10^6, 10^7] \\ t \in [10^7, 3.4\,10^7] \end{array}$
^{32}S	$p_S(t) = \left\{ \begin{array}{l} 2.9e-11 \\ 2.9e3\,t^{-2} \end{array} \right.$	$\begin{array}{l} 2.9e-11 \\ 2.9e3\,t^{-2} \end{array}$	$\begin{array}{l} 1.8e-11 \\ 1.8e3\,t^{-2} \end{array}$	$\begin{array}{l} 6.6e-11 \\ 6.6e3\,t^{-2} \end{array}$	$\begin{array}{l} t \in [3.4\,10^6, 10^7] \\ t \in [10^7, 3.4\,10^7] \end{array}$
^{40}Ca	$p_{Ca}(t) = \left\{ \begin{array}{l} 4.2e-12 \\ 4.2e2\,t^{-2} \end{array} \right.$	$\begin{array}{l} 4.2e-12 \\ 4.2e2\,t^{-2} \end{array}$	$\begin{array}{l} 2.7e-12 \\ 2.7e2\,t^{-2} \end{array}$	$\begin{array}{l} 9.1e-12 \\ 9.1e2\,t^{-2} \end{array}$	$\begin{array}{l} t \in [3.4\,10^6, 10^7] \\ t \in [10^7, 3.4\,10^7] \end{array}$
^{12}C	$p_C(t) = \left\{ \begin{array}{l} 1.2e-10 \\ 1.2e4\,t^{-2} \\ 1.1e-6\,t^{-0.7} - 3e-13 \end{array} \right.$	$\begin{array}{l} 1.2e-10 \\ 1.2e4\,t^{-2} \\ 1.1e-6\,t^{-0.7} - 3e-13 \end{array}$	$\begin{array}{l} 5.8e-11 \\ 5.8e3\,t^{-2} \\ 2.9e-8\,t^{-0.5} - 8e-13 \end{array}$	$\begin{array}{l} 3.6e-10 \\ 3.6e4\,t^{-2} \\ 6.4e-5\,t^{-0.9} - 2e-13 \end{array}$	$\begin{array}{l} t \in [3.4\,10^6, 10^7] \\ t \in [10^7, 3.4\,10^7] \\ t \in [2\,10^8, 5\,10^9] \end{array}$
^{14}N	$p_{Ns}(t) =$	$7.7\,Z_0\,t^{-1.4}$	$0.98\,Z_0\,t^{-1.3}$	$520\,Z_0\,t^{-1.6}$	$t \in [3.4\,10^6, 15\,10^9]$
$p_{Np}(t) = \left\{ \begin{array}{l} Z_0 < 0.004 \\ Z_0 \in [0.004, 0.02] \\ Z_0 > 0.02 \end{array} \right.$	$\begin{array}{l} 3.3e-12 \\ \frac{3.3e-18}{Z_0^{5/2}} \\ 5.8e-14 \end{array}$	$\begin{array}{l} 3.3e-12 \\ \frac{3.3e-18}{Z_0^{5/2}} \\ 5.8e-14 \end{array}$	$\begin{array}{l} 4.6e-12 \\ \frac{4.7e-18}{Z_0^{5/2}} \\ 8.3e-14 \end{array}$	$t \in [10^8, 2.5\,10^8]$	

Table 3. Rate of release of chemical yields of various elements for SSPs of age t and with different IMFs; the rates drop to zero out of the respective time ranges, indicated in the rightmost column. In the case of nitrogen, we distinguish the secondary and the primary components and give metallicity-dependent prescriptions; Z_0 is the initial metallicity of the SSP. Needless to say, the total yield for nitrogen is $p_{\text{N}}(t) = p_{\text{Ns}}(t) + p_{\text{Np}}(t)$ (see text for details).

nett et al. 1999, Henry et al. 2000, Carigi 2000, Liang et al. 2001). Considering these uncertainties, for the purpose of the present chemical algorithm we simply provide carbon yields averaged over metallicity both for massive stars (time range 3.4–34 Myr) and for the delayed contribution of lower mass stars (0.2–5 Gyr). Also for carbon the entries in Table 3 have been adjusted on the base of observational constraints for the Solar Vicinity.

The stellar nucleosynthesis of nitrogen is also complex, and the distinction between its primary and secondary production (Tinsley 1980) is of prime importance to interpret observational evidence (e.g. Larsen et al. 2001 and references therein). For nitrogen, therefore, we consider it worth treating the secondary and primary components separately (p_{Ns} and p_{Np}), with metallicity dependent prescriptions. The secondary component is, by definition, directly proportional to the metallicity of the parent SSP and is produced by stars of all masses (from 3.4 Myr to 15 Gyr). Primary production occurs in intermediate mass stars of 3.5–5 M_{\odot} (time range ~ 100 –250 Myr) and is very sensitive to metallicity, being more efficient at lower metallicities (Marigo 2001, her case $\alpha=1.68$ adopted here). Hence we give a metallicity dependent fit also for the primary component. For carbon and nitrogen, the relative importance of the production by intermediate and low mass stars with respect to that by mas-

sive stars increases when moving from the Arimoto–Yoshii to the Salpeter to the Kroupa IMF, due to the corresponding shift of the SSP towards less massive stars.

The contribution of SN Ia

Table 3 provides the rate of metal release in time from single stars in a SSP of total unit mass. We should then add the contribution of SN Ia, which originate in binary systems. This is easily done since we know the rate of SN Ia in time (Table 2); for each SN Ia, we adopt the chemical ejecta M_Z^{Ia} from the W7 model by Iwamoto et al. (1999). The total metal release by the SSP, including the contribution of SN Ia, is given by:

$$p_Z^{tot}(t) = p_Z(t) + M_Z^{Ia} \times r_{Ia}(t)$$

as listed in Table 4.

Hence, within a timestep Δt a SSP of age t releases an amount of metals given by:

$$\Delta m_Z = \int_t^{t+\Delta t} e_Z(t') dt' = \int_t^{t+\Delta t} p_Z^{tot}(t') dt' + Z_0 \int_t^{t+\Delta t} e(t') dt'$$

or, equivalently, ejects an amount $\int_t^{t+\Delta t} e(t') dt'$ of gas with metallicity:

^{12}C	$p_C^{tot}(t) = p_C(t) + 4.83 \cdot 10^{-2} r_{Ia}(t)$
^{14}N	$p_N^{tot}(t) = p_N(t) + 1.16 \cdot 10^{-6} r_{Ia}(t)$
^{16}O	$p_O^{tot}(t) = p_O(t) + 0.143 r_{Ia}(t)$
^{24}Mg	$p_{Mg}^{tot}(t) = p_{Mg}(t) + 8.5 \cdot 10^{-3} r_{Ia}(t)$
^{28}Si	$p_{Si}^{tot}(t) = p_{Si}(t) + 0.154 r_{Ia}(t)$
^{32}S	$p_S^{tot}(t) = p_S(t) + 8.46 \cdot 10^{-2} r_{Ia}(t)$
^{40}Ca	$p_{Ca}^{tot}(t) = p_{Ca}(t) + 1.19 \cdot 10^{-2} r_{Ia}(t)$
^{56}Fe	$p_{Fe}^{tot}(t) = p_{Fe}(t) + 0.626 r_{Ia}(t)$
Z	$p_Z^{tot}(t) = p_Z(t) + 1.4 r_{Ia}(t)$

Table 4. Total rate of release of chemical yields from a SSP, including the contribution of SN Ia. $r_{Ia}(t)$ is given in Table 2

$$Z_t(\Delta t) = \frac{\Delta m_Z}{\int_t^{t+\Delta t} e(t') dt'} \quad (9)$$

4.3.2 Metal release from the star particle

A particle which has experienced SF is considered to host a SSP, which releases gas and metals in time as calculated above. From the chemical point of view, that is, within such a particle there are “hidden” stellar and gaseous sub-components evolving in time. From the point of view of hydrodynamics, however, in our simulations we do not resolve these sub-components: a baryonic particle is labelled either as gas or as star, and behaves accordingly either as collisional or collisionless matter. We must hence translate the chemical enrichment of a SSP calculated above into chemical enrichment of the gas particles.

Just as in the case of gas restitution and of the SN rates (§4.1 and §4.2), we resort to a statistical approach. A particle which has experienced SF may either remain a star forever, or become at some point a gas–again particle. As long as it remains a star particle, it is assigned the metallicity Z_0 of its SSP; when at some timestep Δt it turns into a gas–again particle, it is assigned the composition $Z_t(\Delta t)$ of the gas released by the SSP within Δt , given by (9).

Once more, the main limit of this approach may reside in poor statistics: the metal production of a whole stellar population is sampled by the, possibly small, fraction of it which dies within the timestep Δt . A large enough number of particles is necessary to obtain a meaningful statistical sampling, and the “chemical timestep” must be chosen appropriately, generally longer than the hydro–dynamical timestep (see §4.2.3). Our test for the single burst case and our simulations below indicate that our algorithm works already with a few thousand baryonic particles.

4.4 Metal diffusion in the gas

Finally, we must describe the chemical evolution of the overall population of gas particles, both gas–again particles and those which have never been stars, which proceeds by metal diffusion. Particles which were never stars can acquire metals from neighbouring gas–again particles through diffusion.

Conversely, a gas–again particle is initially assigned the metallicity $Z_t(\Delta t)$ from Eq. (9) as discussed above; from then on, its composition will evolve only by metal exchange with other nearby gas particles, with no further memory that it had been a star in the past. For the sake of metal diffusion, that is, once the initial metallicity of a gas–again particle has been assigned there is no need to distinguish between gas and gas–again particles.

At each time step, we diffuse metallicity among gas particles according to the scheme originally developed by Groom (1997), which consists of an SPH translation of the usual diffusion equation:

$$\frac{dZ}{dt} = -\kappa \nabla^2 Z \quad (10)$$

where κ is the diffusion coefficient. In principle, this scheme is more physically grounded than the widely used SPH-smoothing, in which metals are SPH-spread among the neighbouring particles. It relies on the idea that the diffusion of metals is driven by SN explosion and energy injection in the interstellar medium during the SN remnant phase.

We derive the diffusion coefficient from the models by Thornton et al. (1998). The typical size of a SN remnant after 10^6 yr from the explosion is 50–100 pc, whereas the typical velocity of the gas accelerated by the SN remnant at that time is 40–60 km/sec. In this way we obtain:

$$\kappa = (50 \text{ km sec}^{-1})(1.85 \times 10^{15} \text{ km}) \text{ km}^2 \text{ sec}^{-1}$$

The SPH translation, which requires second derivatives of the kernel, is

$$\frac{dZ_i}{dt} = - \sum_{j=1}^N \kappa m_j \left(\frac{2}{\rho_j + \rho_i} \right) (Z_i - Z_j) \times |\nabla^2 W_{ij}(|\vec{r}_i - \vec{r}_j|, h_{ij})| \quad (11)$$

This SPH algorithm was successfully tested by Groom (1997) versus suitable analytical exact counterparts.

A possible drawback of the adopted diffusion scheme could be the use of the 2^{nd} derivative of the smoothing function, which may introduce spurious fluctuations in the resulting metallicity. The use of a spline kernel, which is continuous with its 1^{st} and 2^{nd} order derivatives, ensures that unphysical fluctuations in the diffused quantities (metallicity in our case) do not appear.

5 A SINGLE BURST

A first useful test for our algorithm is to model the evolution of the various chemical quantities (gas fraction, metallicity etc.) in the simple case of a single burst of SF. This test focuses entirely on the implemented chemical network, uncoupled in this case from hydrodynamical effects. It allows us on one hand to visualize the expected chemical production of a SSP, and on the other hand to check the validity of the statistical approach.

The single burst model is realized with 5000 particles of gas, of total mass of $10^{11} M_\odot$, turned into stars instantaneously at the beginning of the simulation ($T_0 = 0$, $Z_0 = 0$). These star particles are let evolve afterwards according to the statistical prescriptions for gas and metal restitution given above, without any further SF episodes.

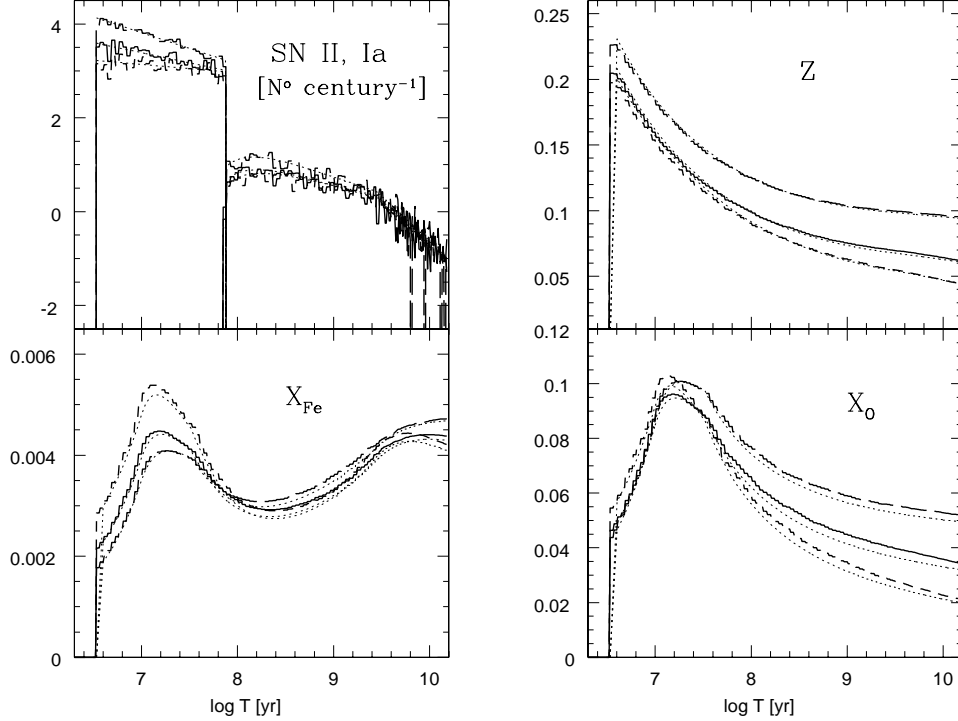


Figure 5. Chemical evolution for a single burst of star formation involving $10^{11} M_{\odot}$. *Upper-left panel:* cumulative rates of SN II and Ia ($T <$ and $> 7.5e7$ yr, respectively) in logarithm of the number of events per century. *Upper-right panel:* evolution of the total metallicity. *Lower panels:* evolution of iron (on the left) and oxygen (on the right) abundances. *Solid line:* numerical results for the Salpeter IMF; *short-dashedline:* Kroupa IMF; *long-dashed line:* Arimoto-Yoshii IMF. The *dotted lines* are the corresponding exact analytical predictions.

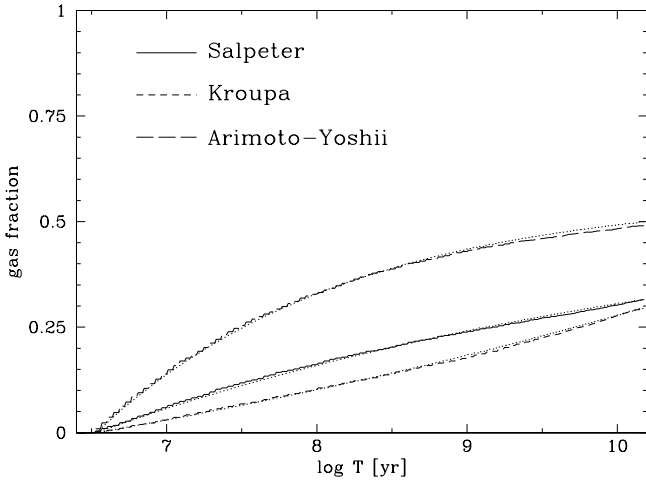


Figure 4. Returned gas fraction in time for a single burst of star formation involving 5000 particles. Thin dotted lines represent the exact analytical expectations.

It is sufficient to model the evolution of a couple of characteristic elements with different production timescales, to assess the capability of the statistical approach in describing detailed chemical evolution in time. We choose to follow the evolution of oxygen (representative of α -elements produced

by massive stars over short time scales), of iron (representative of elements with a delayed contribution), and of the global metallicity.

As everything in our algorithm (SN rates, metal production etc.) is entirely governed by the statistical gas restitution, it is fundamental to check this quantity first of all. Fig. 4 shows the evolution of the returned gas fraction in time for our single burst test, for the three IMF cases, as compared to the exact expectations computed directly from the analytical fitting functions. The response of the algorithm is very good already with ~ 5000 particles.

In Fig. 5 we display the results for SN rates and for the evolution of metallicity, iron and oxygen abundances in the returned gas, again compared to the analytical predictions.

The results reproduce the expected trends for a SSP, and although statistical fluctuations are apparent, for instance, in the predicted SN rates, the overall behaviour is traced quite well. Metallicity is very high at the beginning, when the highly metal enriched gas from massive stars is expelled. Later, this extremely metal rich gas is diluted by more metal poor gas ejected by long-lived stars, so that metallicity decreases. The oxygen abundance follows the same trend, and represents roughly a half of the global metallicity, being oxygen in fact the most abundant of all metals. The iron abundance also decreases after the initial peak due to massive stars, but contrary to oxygen it later stabilizes and even increases again thanks to the contribution of SN Ia. The oxygen-to-iron ratio correspondingly

changes from super-solar values at early times, when SN II dominate the chemical enrichment, to solar and sub-solar values at later times.

The absolute number of SN is largest for the Arimoto–Yoshii IMF, which is the most top-heavy, and decreases moving to the Salpeter and to the Kroupa case; the same trend is seen in the respective metallicities and oxygen abundances, dominated by the production of massive stars. The *relative* number of SN Ia to SN II, however, decreases when going from Arimoto–Yoshii to Salpeter to Kroupa because these latter IMFs are more skewed toward smaller stellar masses. Hence, the final $[O/Fe]$ ratio typical of the Arimoto–Yoshii SSP is larger than for the other IMF cases.

Within the range of massive stars ($T \lesssim 10^8$ yr), one can notice that the typical iron abundance in the ejected gas increases going from the Arimoto–Yoshii to the Salpeter to the Kroupa IMF. This is due to the fact that SN from progenitors in the low mass end of massive stars (say, $8-15 M_{\odot}$) are expected to produce a higher amount of iron, relative to the global mass ejection or to the oxygen production, than stars in the higher mass range. Hence, the Arimoto–Yoshii IMF favours the highest masses with very oxygen-rich, and less iron-rich, ejecta; on the contrary, the Kroupa IMF is more skewed toward SN with a higher relative iron production. As a consequence, the typical $[O/Fe]$ ratio of SN II ejecta from an Arimoto–Yoshii SSP is higher than from a Salpeter SSP than for a Kroupa SSP. Typical values are $[O/Fe]=+0.56$ for Arimoto–Yoshii, $+0.50$ for Salpeter, $+0.45$ for Kroupa. The theoretical estimates of iron production as a function of mass, on the other hand, are very uncertain and this detailed mass effect might be somewhat spurious. However, all of these values are compatible with empirical evidence for the α -enhanced stellar population of the Galactic halo (see e.g. the data by Carretta et al. 2000 in Fig. 11).

The Kroupa IMF has been adopted for the simulations presented in the following.

6 A DISC-LIKE GALAXY

As a first astrophysical test-application of our code we run a simulation for an individual galaxy.

The initial configuration for this object is a spherical DM halo with a density profile $\propto 1/r$ (see Lia et al. 2000 for a justification of this choice). The total mass of the system is $1.3 \cdot 10^{12} M_{\odot}$ with a baryonic fraction equal to 0.1. The galaxy is modeled using 30,000 baryonic particles and 15,000 DM particles. Accordingly, the mass of a DM particle is $7.8 \times 10^7 M_{\odot}$, while the mass of a gas particle is $4.3 \times 10^6 M_{\odot}$. We assign to the halo a rigid rotation with an angular speed $\lambda = 0.08$.

Due to both cooling and angular momentum, gas cools down in a thin rotating disk forming stars. The distribution of star and gas particles are shown in Fig. 6. The snapshots refer to 7 Gyr from the beginning of the simulations; while star particles are settled into a stellar disc-like object, most of the gas is in the form of a hot spheroidal halo.

In Fig. 7 we plot the SF history (SFH) of the overall object (solid line). The SFR exhibits a strong peak in the initial 0.5 Gyrs, then sharply declines and by the age of 4 Gyrs settles to a rather low constant value of a few M_{\odot}/yr . Correspondingly, in the final Gyrs of the simulation most of

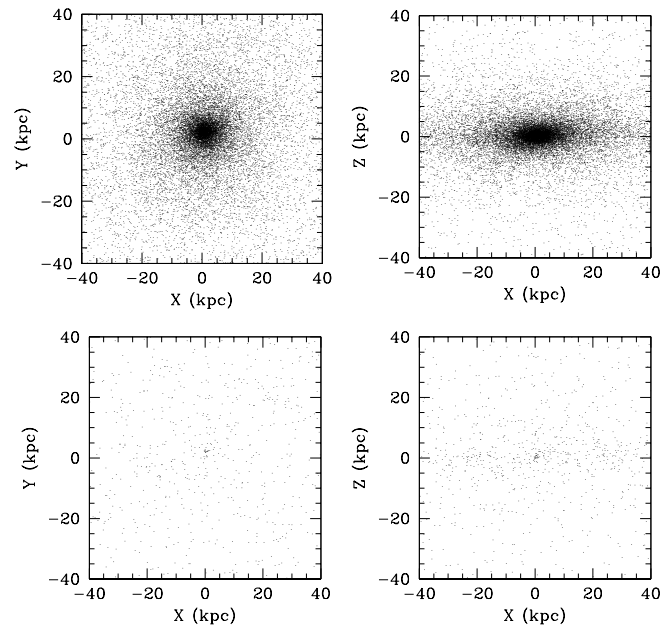


Figure 6. Distribution in the x-y and x-z planes of star particles (*top panels*) and of gas particles (*bottom panels*) in the innermost 40 kpc, after 7 Gyrs.

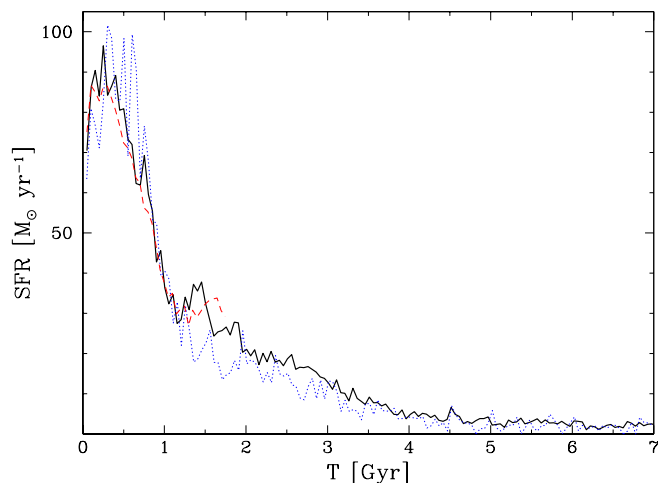


Figure 7. Global star formation history of our disc-like galaxy. The thin dotted and dashed lines correspond to the low resolution and very high resolution simulations, respectively.

the gas is distributed in a rather hot halo (Fig. 6) around the stellar disc, while little cold gas is left to fuel more active SF within the disc.

To test the behaviour of the “chemical algorithm” in the simulation, we compare it with the results of a detailed one-zone chemical evolution model with the same SFH: global properties like the overall gas consumption, SN rates etc. should correspond. Usually, models for chemical evolution calculate their own SFH internally after some prescribed analytical Schmidt-like law (e.g. Portinari & Chiosi 1999). For the present purpose, we developed instead a version of

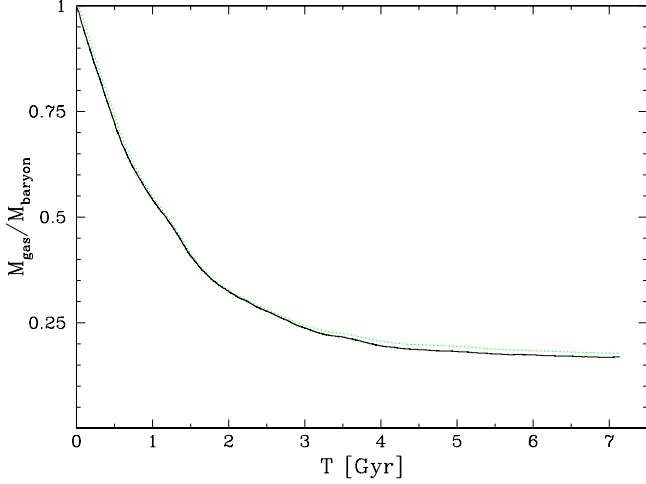


Figure 8. Evolution of the global gas fraction in our disc-like galaxy (*solid line*) compared to the predictions of a detailed chemical model (*dotted line*).

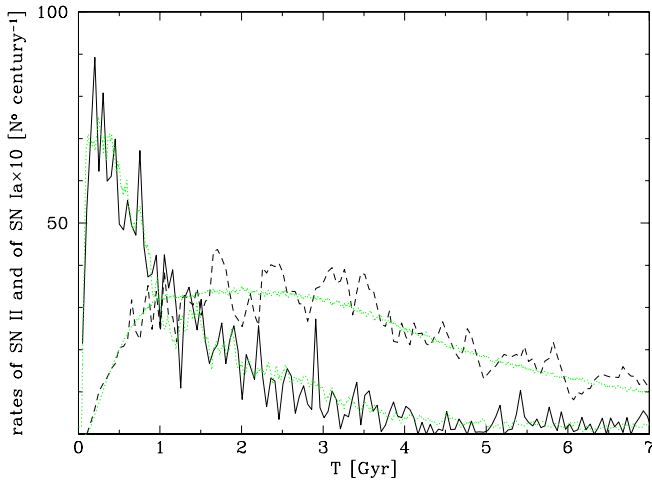


Figure 9. Evolution of the SN rates. *Solid line*: type II SN; *dashed line*: type Ia SN (rate amplified by a factor of 10 for the sake of clarity); *dotted lines*: corresponding predictions from the chemical model.

the chemical model by PCB98 suitable to be force-fed the SFH as an input information. The chemical model has then been run for a closed system, just as our hydro-dynamical galaxy is when considered globally.

Fig. 8 shows the evolution of the global gas fraction in our object, as SF proceeds. The dotted line is the corresponding prediction from the chemical model, once the SFH in Fig. 7 is imposed. The agreement is quite good.

Fig. 9 shows the time evolution of the SN rates for type II and type Ia SN, respectively. Notice how the rate of SN II closely traces the SFR, as expected, while the rate of SN Ia is much more diluted in time. In this object with a low final SFR, the two types of SN end up with comparable rates. The trend for the SN rates, just as for the gas consumption in the previous figure, is in full agreement with the predictions of the chemical model; this is a confirmation

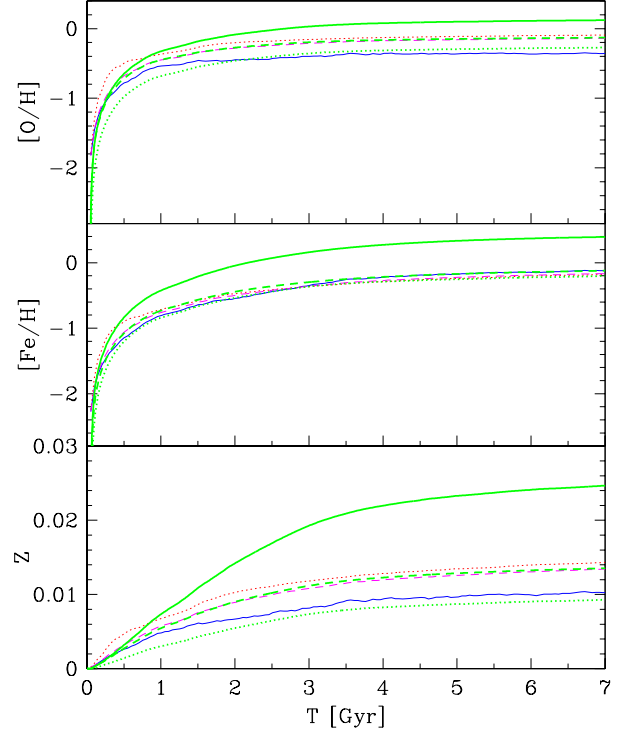


Figure 10. Global (gas+stars) average metal enrichment history (*dashed lines*) and for gas and stars separately (*solid and dotted lines*, respectively). *Thin lines*: SPH simulation; *thick lines*: one-zone chemical model. The global average metal enrichment compares very well between the two models (see text).

of the good behaviour of our algorithm for gas restitution and chemical evolution in more complex simulations than a single burst.

With respect to the detailed metallicity evolution of the gaseous and stellar components of the system, instead, it is little meaningful to compare the hydrodynamical simulation and the one-zone chemical model. In fact, a basic assumption of one-zone models is that the system is always homogeneous in space, namely the metals produced and ejected by stars are instantaneously mixed and spread over the whole gas mass in the system. This is fundamentally different from the behaviour of dynamical models of galaxies, where star formation and metal pollution are localized. In a realistic disc-like galaxy stars pollute, and form from, the gas in the disc region, while there will be a fraction of gas away from the disc which may take little or no part to SF and metal pollution. Qualitatively, in a dynamical simulation of a disc galaxy we expect stars to enrich a more limited amount of gas (that located in their surroundings), which gets enriched more effectively than in the one-zone model; this highly enriched gas is somehow “compensated” by the the pristine, or almost pristine, gas residing far away from the disc. Consequently, the stars in the disc form in an environment which is more metal enriched than what a simple one-zone model predicts, and their metallicity distribution is expected to be different than that derived from the chemical model. However, if the distribution of metals between gas and stars is

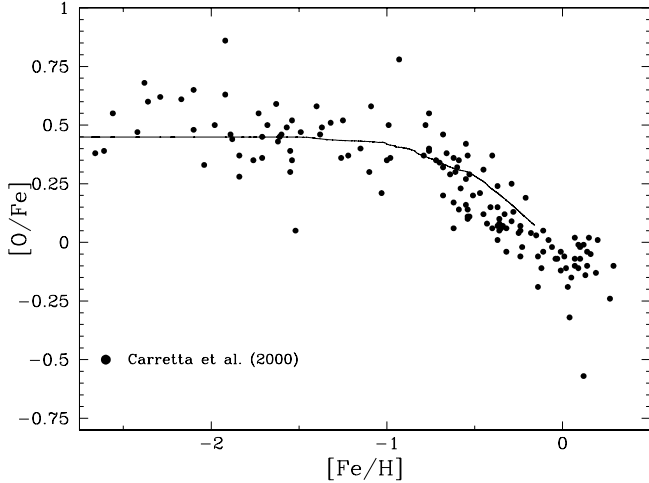


Figure 11. Evolution of the average chemical composition of the stellar component: $[\text{O}/\text{Fe}]$ ratio versus metallicity

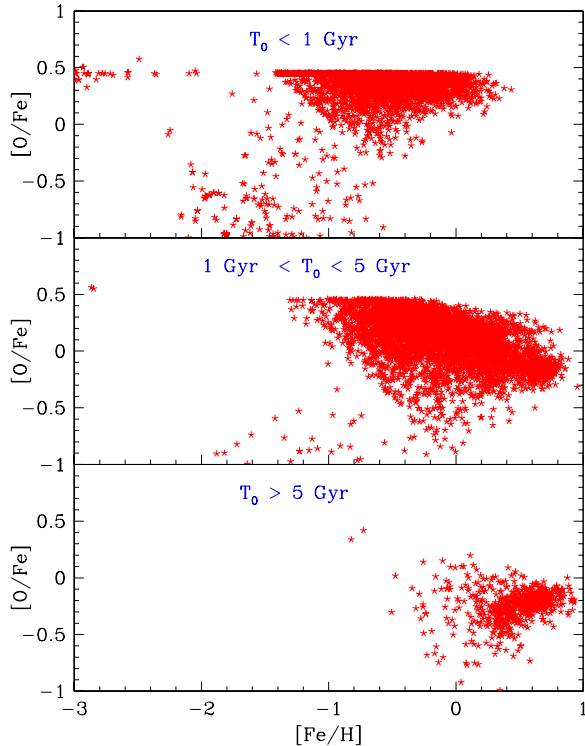


Figure 12. Chemical composition of stars in three different age bins (old, intermediate and young). T_0 is the birth time of stars, the overall system is 7 Gyr old.

expected to be different in the dynamical simulation and in the chemical model, the global metallicity of the *sum* of the gaseous+stellar components should be comparable between the two models, as this traces the global metal production for that particular SFH. Fig. 10 illustrates these expected effects: the histories of metal enrichment for gas and stars separately are evidently very different between the one-zone model and the simulation. In particular, in

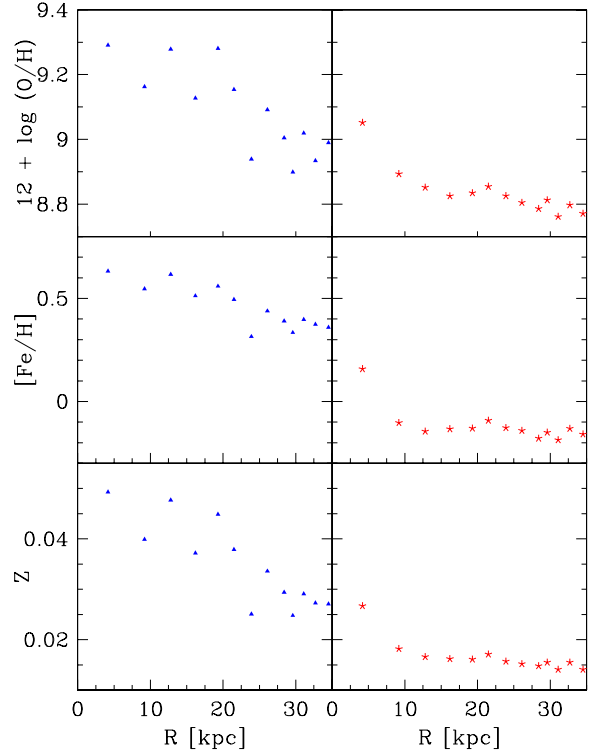


Figure 13. Metallicity profiles for gas (left panels) and stars (right panels)

the hydro-dynamical simulation more metals result locked into the stellar component, since the stars form in localized, very metal enriched regions; correspondingly, the gas metallicity in the overall is lower than that of stars because the gas component includes also plenty of un-processed hot gas in the outskirts of the galaxy. However, when one considers the global metal enrichment (dashed lines, average of gas+stars), which is the record of the overall metal production, the two models compare very well; minor differences can be imputed to the fact that the chemical model by PCB98 includes detailed metallicity-dependent yields, while our fitting formulæ in Table 3 are based on average values of the yields. The comparison in Fig. 10 implies that the chemical algorithm in the SPH simulation gives an adequate description of the metal production.

Fig. 11 shows the evolution of the global, average $[\text{O}/\text{Fe}]$ ratio for the stellar component, versus metallicity. At low metallicities stars display an α -enhanced composition typical of SN II enrichment, while at higher metallicities the $[\text{O}/\text{Fe}]$ ratio decreases, as expected from the additional contribution of SN Ia to the iron production. Notice how the predicted evolution compares to the observational data for stars in the Solar Neighbourhood. We remark, however, that this comparison must be regarded only as qualitative, since the present simulation is not aimed at reproducing the Milky Way or the Solar Neighbourhood, but only to test the self-consistency of the chemical algorithm we implemented. Actually, our object in the end resembles more the gas-consumed disc of a young S0 than that of an Sb spiral like our own Galaxy.

Fig. 12 shows the chemical composition of stars in three representative age bins: “old” stars born within the first Gyr of the simulation, “intermediate age” stars, born between 1 and 5 Gyrs of the simulation, and “young” stars, i.e. younger than 2 Gyr by the end of the simulation. As expected, the bulk of old stars concentrate around high $[O/Fe]$ ratios because little iron has yet been contributed by SN Ia, while at decreasing age the bulk of stars moves to higher metallicities and lower $[O/Fe]$ ratios. The stars of the youngest bin end up with super-solar metallicity and slightly under-solar $[\alpha/Fe]$ composition.

Finally, in Fig. 13 we show the metallicity profiles, for gas and stars, in the innermost regions at the final age of 7 Gyr. In these regions, where the bulk of the galaxy resides, the gas is much more metal rich than the stars, as expected in general since the gas is an instantaneous picture of the chemical enrichment reached at present, while stars are a signature of the accumulated chemical history starting from the initial, metal-poor early epochs. Besides, in the galaxy under examination very little gas is left in the late stages within the stellar disc, hence its chemical enrichment proceeds very fast.

Metallicity gradients are visible, and they are more pronounced for the gas component than for the stars, as expected in general from chemical evolution models (e.g. Edmunds & Greenhow 1995).

6.1 Testing the effects of resolution

A basic issue of hydrodynamical simulations of galaxy formation is to what extent the results are affected by resolution. In principle, this problem might be even more crucial when a statistical algorithm is used for SF and chemical evolution.

The resolution effect on the SFH of individual galaxies has been explored in Lia et al. (2000) by means of *ad hoc* simulations of the same individual galaxy at increasing number of particles (2,000, 20,000 and 200,000). They showed that the SF recipe converged above 20,000 particles; beyond that, the SFH did not change significantly by varying the particle number further.

We repeat an analogous test here for our disc-like galaxy, since our SF algorithm is different now: although we adopt the same formal SF law as in Lia et al. (2000), this law is now implemented with a probabilistic approach (§ 3). Besides, resolution tests are needed not only for the convergence of the SFH, but also because the gas and metal restitution are treated statistically.

In the previous section, we discussed the self-consistency of our chemical algorithm for a simulation with 30,000 baryonic particles, by comparing its results with a one-zone chemical model, where possible. We will refer to this simulation as the “high-resolution” one. Fig. 7 also shows the SFH of the same galaxy modelled with “low resolution” (8,000 particles, thin dotted line) and with “very high resolution” (200,000 particles, thin dashed line).

The low resolution case shows a much more noisy SFH, although qualitatively the trend resembles that of the high resolution case: an initial high SFR is maintained for ~ 1 Gyr, after that its level declines rapidly.

Fig. 14 illustrates the performance of the chemical algorithm in the low resolutions case. The gas restitution (top

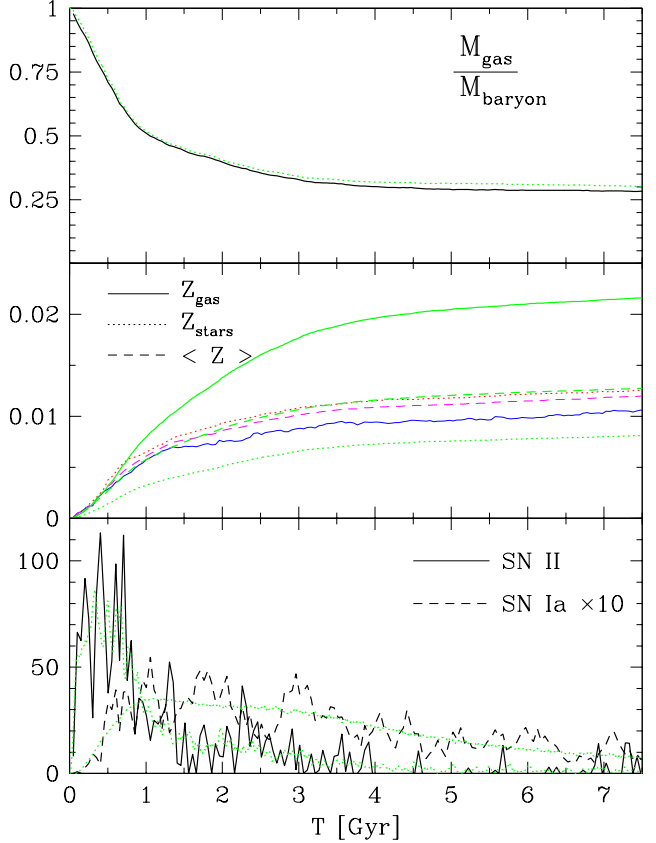


Figure 14. Comparison between the low resolution galaxy simulation and the chemical one-zone model with the same SFH (the dashed line in Fig. 7). *Top panel:* evolution of the gas fraction; solid and dotted lines for simulation and chemical model respectively, as in Fig. 8. *Mid panel:* metallicity evolution for gas, stars and global average; thin and thick lines for simulation and chemical model respectively, as in Fig. 10. *Bottom panel:* evolution of the SN rates; the dotted lines are the predictions of the chemical model.

panel), and consequently the metal release (mid panel), are a bit underestimated when compared to the predictions of the one-zone model. This can be imputed to the large oscillations of the SFR; these oscillations produce even stronger noise in the gas (and metal and SN) release, as these imply a further “probabilistic event” on top of the one that induces SF. This noise is particularly evident in the SN rates (bottom panel). However, the effect is not large: gas and metal restitution seems to be underestimated just by 10% or so. Also the SN rates in the simulation, in spite of heavy oscillations, on average follow the exact one-zone counterpart.

The very high resolution simulation was followed up to 1.75 Gyr, with the sole purpose of demonstrating that the SFH converges when the number of particles is increased beyond 30,000. As the performances of the chemical algorithm are very good in the high resolution simulation (see previous section), once the convergence of the SFH is also demonstrated one can be confident about the overall consistency of the results.

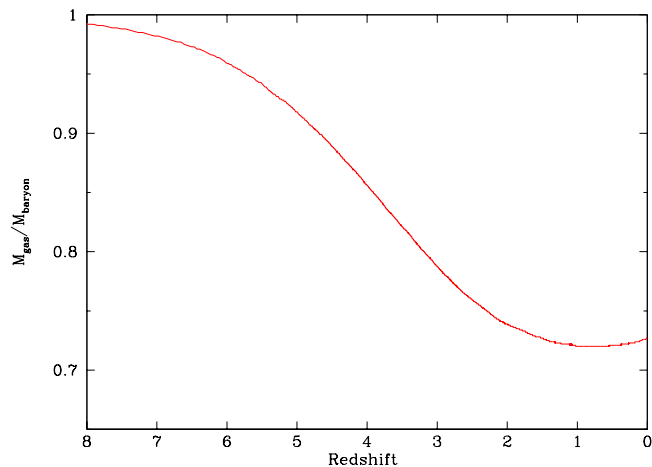


Figure 15. Evolution of the global gas fraction in the cluster

In summary, concerning resolution effects we can conclude the following.

- With 8,000 particles the SFH and chemical evolution of the object are quite noisy, and the statistical algorithm somewhat underestimates the gas and metal release. However, for that SFH the mismatch with respect to the detailed chemical model is by no means dramatic (within 10%) so the gross features of chemical evolution are already rendered.
- With 30,000 particles and beyond, the SFH converges and at that level of resolution the statistical chemical algorithm also responds pretty well.

Concerning this latter point, a similar result was found by Lia et al. (2000): the SFH in their simulations converged beyond 20,000 particles. Since in their case the SF law itself are dominant, while the probabilistic approach has a minor impact on the resolution limit. Most important, we stress once more that beyond the resolution limit for the SFH, also the statistical chemical algorithm for gas and metal restitution performs very well.

7 A CLUSTER OF GALAXIES

Other interesting astrophysical applications of chemohydrodynamical codes lie in cosmological simulations of the formation and evolution of clusters, to address the problem of the chemical enrichment of the ICM self-consistently. For the sake of example, we present here one such simulation.

The initial conditions were realized by perturbing a cubic grid of particles with the displacements field made available by the *Cluster Comparison Project* (<http://star-www.dur.ac.uk/csf/clusdata/>). The initial fluctuation spectrum was taken to have an asymptotic spectral index, $n = 1$, and shape parameter, $\Gamma = 0.25$; the cosmological parameters assumed were: mean density, $\Omega = 1$; Hubble constant, $H_0 = 50 \text{ km s}^{-1} \text{ Mpc}^{-1}$; present-day linear rms mass fluctuations in spherical top hat spheres of radius 16 Mpc , $\sigma_8 = 0.9$; and baryon density (in unit of the critical density), $\Omega_b = 0.1$. The perturbation was centered on a cubic region of size $L = 64 \text{ Mpc}$. See Frenk et al. (1999) for

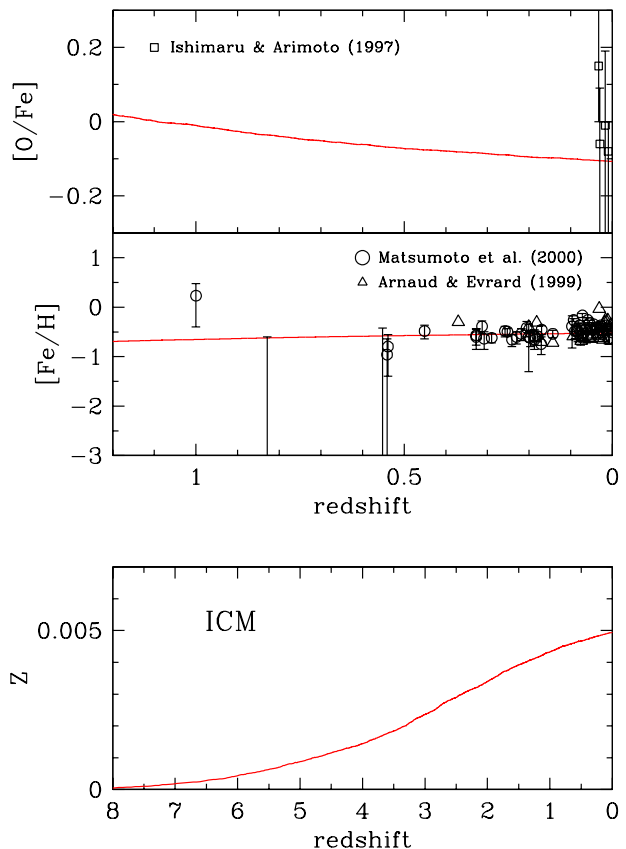


Figure 16. Chemical enrichment in time for the ICM

more details. The system was divided in two zones, an inner sphere of radius 22 Mpc which was filled with 36^3 gas particles and 36^3 dark particles, surrounded by a sphere of radius 32 Mpc in which only dark matter was present. Initially gas and dark matter were placed on top of each other and were given the same velocities, computed using the Zel'dovich approximation and adding the Hubble flow. In the inner region the masses of a DM and gas particle are $2.1 \times 10^{10} M_\odot$ and $2.4 \times 10^9 M_\odot$, respectively.

Fig. 15 shows the evolution of the gas fraction over the total baryonic matter. At the end of the simulation, $\sim 75\%$ of the baryons are in gaseous form, while 25% is locked into stars, compatible with observed estimates (the mass in gas in clusters is 2–5 times that in galaxies, Arnaud et al. 1992).

Fig. 16 shows the evolution of chemical abundances in the gaseous component. The final metallicity in the ICM is ~ 0.25 solar, in broad agreement with observational values. Notice how the metallicity evolution in the gas is negligible at low redshifts ($z < 1$), consistent with observational data (Mushotzky & Loewenstein 1997, Matsumoto et al. 2000). Also the average $[\text{O}/\text{Fe}]$ ratio is compatible with observational data, although these are highly uncertain (Ishimaru & Arimoto 1997).

Fig. 17 shows the final metallicity distribution in the ICM. A hint of the existence of a metallicity gradient (a recent “hot” issue, De Grandi & Molendi 2001, Finoguenov et al. 2000, White 2000) can be seen in Z and in $[\text{Fe}/\text{H}]$.

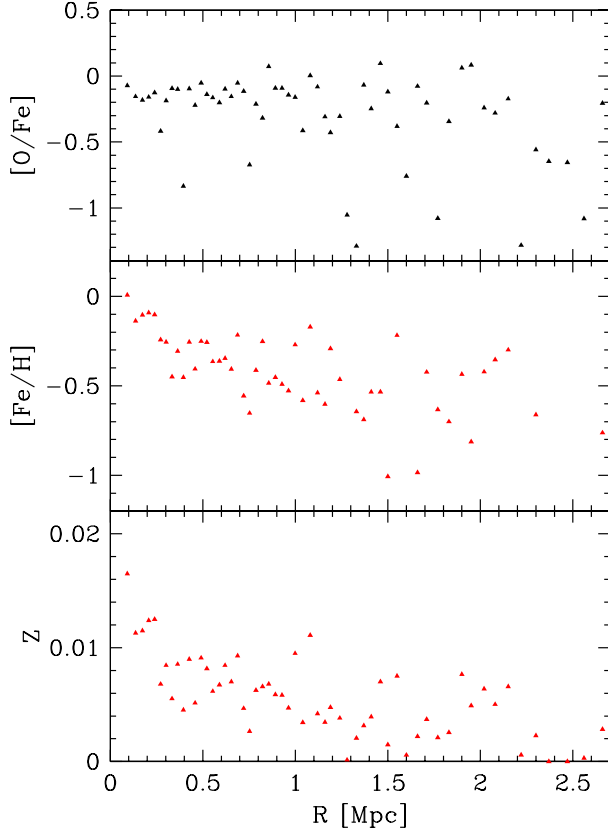


Figure 17. Metallicity gradients for gas in the ICM

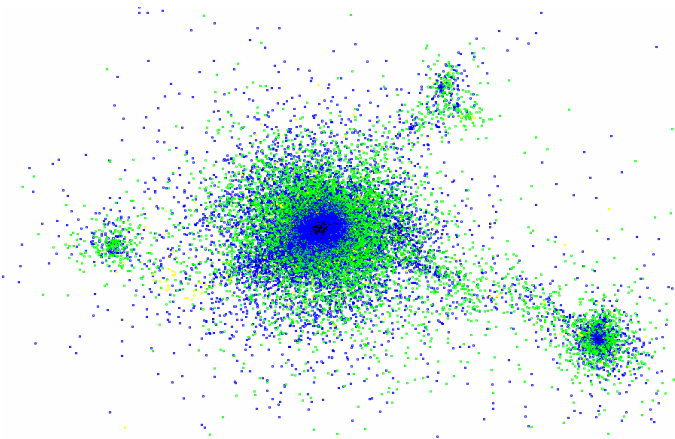


Figure 18. Iron distribution in the ICM: the darkest regions indicate zones with higher iron content. See fig.17 for comparison

In particular, a metallicity peak can be distinguished in the very central regions (200–300 kpc), while further out metallicity seems to be more uniformly distributed, though with a large scatter. Concerning the radial behaviour of the $[\alpha/\text{Fe}]$ ratio, in our simulation there seems to be no differential gradients for α -elements and iron, as the $[\text{O}/\text{Fe}]$ ratio seems to be roughly uniform at all radii, with slightly subsolar values,

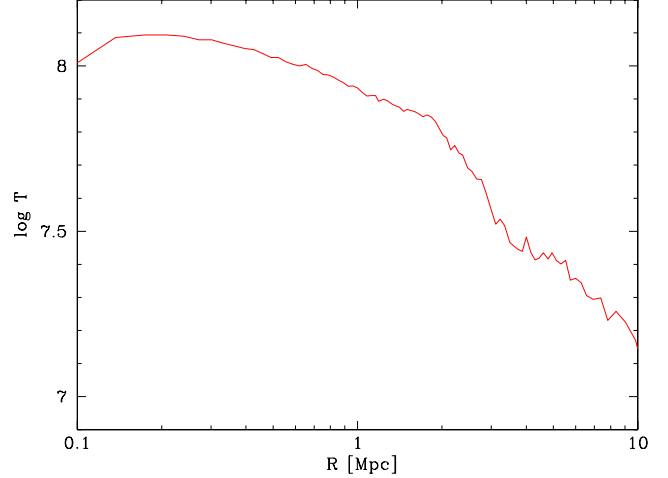


Figure 19. Radial temperature profile for the gas in the ICM

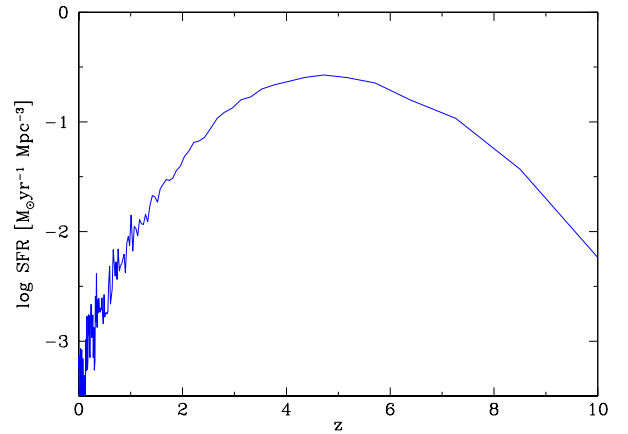


Figure 20. Global star formation history per unit volume from the whole simulation

though with a large scatter. The iron distribution is shown in Fig. 18, while the temperature profile is plotted in Fig. 19.

Finally, in Fig. 20 we show the estimated average evolution of the SFR per Mpc^3 for the global simulation. Notice how the peak on the SFR is more intense and located at earlier phases ($z \sim 5$) with respect to what observed in the field (e.g. Madau et al. 1996, Steidel et al. 1999). This is in line with expectations when looking at areas of larger density than average; in fact, in our simulation we are dealing with a slice of Universe where the formation of a cluster of galaxies takes place.

Higher resolution simulations are needed to assess this problem in the necessary detail, resolving also e.g. the gas still bound to individual objects from that actually expelled into the ICM, the role of ram pressure stripping over individual galaxies in the central parts of the cluster, and so forth. Such higher resolution simulations will be addressed in future work. In the context of the present paper, we presented this simulation here mostly for illustration purposes, with no claims of conclusiveness.

8 SUMMARY AND CONCLUSIONS

In this paper we developed a new algorithm for detailed calculation of chemical evolution in SPH codes, conceived so as to be implemented with minor computational costs into simulations with a very large number of particles, and in parallel codes. As computer power and capabilities continue to improve, allowing for heavier and heavier simulations, the opportunity arises to develop algorithms for the “astrophysical calculations” (star formation, chemical evolution etc.) which provide increasing accuracy the larger the number of particles involved. At the same time, as the heaviest computational effort is typically devoted to the calculation of gravity forces, these “astrophysical” algorithms should bear as least as possible on the performances, maintaining a low relative computational load when the number of particles increases. Our statistical algorithm for star formation and chemical evolution, presented in this paper, is specifically addressed to this purpose.

After testing the self-consistency of the algorithm, with two illustrative applications we showed how our statistical algorithm, implemented in a SPH code, is suitable to model the evolution and distribution of different chemical elements in various contexts. It provides a tool to follow both the chemo-hydrodynamical evolution of individual galaxies and, in the framework of cosmological simulations, the chemical enrichment of the ICM/IGM as well as the global SFR and cosmic chemical evolution. Besides, the description of star particles as independent SSPs of assigned IMF, age and metallicity should make it straightforward to follow spectro-photometric evolution as well, in the simulations.

Our algorithm is meant to be easy to implement into any SPH code.

ACKNOWLEDGEMENTS

CL thanks C.S. Frenk for fruitful conversations and the kind hospitality during his visit to Durham University. LP acknowledges useful discussions with Jesper Sommer-Larsen, and thanks SISSA/ISAS in Trieste and the Observatory of Helsinki for kind hospitality on various visits. We are also grateful to Claudio Dalla Vecchia for his help in handling the simulations. An anonymous referee is acknowledged for detailed remarks on the first version of the manuscript. This study was financed by the Italian MURST (PhD and post-doc fellowships, and grant Cofin-9802192401) and by the Danmarks Grundforskningsfond (TAC fellowship).

REFERENCES

- Arimoto N., Yoshii Y., 1987, *A&A* 173, 23
 Arnaud M., Evrard A.E., 1999, *MNRAS* 305, 631
 Arnaud M., Rothenflug R., Boulade O., Vigroux L., Vangioni-Flam E., 1992, *A&A* 254, 49
 Barnes J., Hut P., 1986, *Nature* 324, 446
 Berczik P., 1999, *A&A*, 348, 371
 Buonomo F., Carraro G., Chiosi C., Lia C., 2000, *MNRAS* 312, 371
 Burkert A., Hensler G., 1988, *A&A* 199, 131
 Burkert A., Truran J.W., Hensler G., 1992, *ApJ* 391, 651
 Carigi L., 2000, *RMxAA* 36, 171
 Carraro G., Lia C., Chiosi C., 1998, *MNRAS* 297, 1021
 Carretta E., Gratton R.G., Sneden C., 2000, *A&A* 356, 238
 Cen R., Ostryker J.P., 1999, *ApJ* 519, L109
 Chiappini C., Matteucci F., Beers T.C., Nomoto K., 1999, *ApJ* 515, 226
 Chiosi C., 2000, *A&A* 364, 423
 Chiosi C., Bressan A., Portinari L., Tantalo R., 1998, *A&A*, 339, 355
 De Grandi S., Molendi S., 2001, *ApJ* 551, 153
 Dalla Vecchia C., 2001, Master Thesis, Padova University
 Edmunds M.G., Greenhow R.M., 1995, *MNRAS* 272, 241
 Ferrara A., Pettini M., Shchekinov Y., 2000, *MNRAS*, 319, 539
 Finoguenov A., David L.P., Ponman T.J., 2000, *ApJ* 544, 188
 Frenk C.S., White S.D.M., Bode P., et al., 1999, *ApJ* 525, 554
 Garnett D.R., Shields G.A., Peimbert M., et al., 1999, *ApJ* 513, 168
 Gingold R.A., Monaghan J.J., 1977, *MNRAS* 181, 375
 Greggio L., Renzini A., 1983, *A&A* 118, 217 (GR83)
 Groom W., 1997, PhD thesis, Cambridge University
 Gustafsson B., Karlsson T., Olsson E., Edvardsson B., Ryde N., 1999, *A&A* 342, 426
 Henry R.B.C., Edmunds M.G., Köppen J., 2000, *ApJ* 541, 660
 Ishimaru Y., Arimoto N., 1997, *PASJ* 49, 1
 Iwamoto K., Brachwitz F., Nomoto K., et al., 1999, *ApJS* 125, 439
 Jungwiert B., Combes F., Palouš J., 2001, *A&A* 376, 85
 Katz N., Gunn J.E., 1991, *ApJ* 377, 365
 Katz N., Weinberg D.H., Hernquist L.E., 1996, *ApJS*, 105, 19
 Kennicutt R.C., Tamblyn P., Congdon C.W., 1994, *ApJ* 435, 22
 Kroupa P., 1998, *MNRAS* 298, 231
 Larsen T.I., Sommer-Larsen J., Pagel B.E.J., 2001, *MNRAS* 323, 555
 Lia C., 2000, PhD Thesis, SISSA/ISAS, Trieste
 Lia C., Carraro G., 2000, *MNRAS* 314, 145
 Lia C., Carraro G., Salucci P., 2000, *A&A* 360, 76
 Lia C., Dalla Vecchia C., Carraro G., 2001, in “Science and Computing at Cineca - 2000 Report”, in press
 Liang Y.C., Zhao G., Shi J.R., 2001, *A&A* 374, 936
 Lucy L., 1977, *AJ*, 82, 1013
 Madau P., Ferguson H.C., Dickinson M.E., et al., 1996, *MNRAS* 283, 1388
 Maeder A., 1992, *A&A* 264, 105
 Marigo P., 2001, *A&A* 370, 194
 Matsumoto H., Tsuru T.G., Fukazawa Y., Hattori M., Davis D.S., 2000, *PASJ* 52, 153
 Mosconi M.B., Tissera P.B., Cora S.A., Lambas D.G., 2001, *MNRAS*, 325, 34
 Mushotzky R.F., Loewenstein M., 1997, *ApJ* 481, L63
 Portinari L., Chiosi C., 1999, *A&A* 350, 827
 Portinari L., Chiosi C., Bressan A., 1998, *A&A* 334, 505 (PCB98)
 Prantzos N., Vangioni-Flam E., Chauveau S., 1994, *A&A* 285, 132
 Raiteri C.M., Villata M., Navarro J.F., 1996, *A&A* 315, 105
 Recchi S., Matteucci F., D’Ercole A., 2001, *MNRAS* 322, 800
 Samland M., Hensler G., Theis C., 1997, *ApJ* 476, 544
 Salpeter E.E., 1955, *ApJ* 121, 161
 Scalo J., 1998, *ASP Conf. Ser.* 142, 201
 Schmidt M., 1959, *ApJ*, 129, 243
 Steidel C.C., Adelberger K.L., Giavalisco M., Dickinson M., Pettini M., 1999, *ApJ* 519, 1
 Steinmetz M., Müller E., 1994, *A&A*, 281, L97
 Sutherland R.S., Dopita M.A., 1993, *ApJS* 88, 253
 Theis C., Burkert A., Hensler G., 1992, *A&A* 265, 465
 Thomas D., Greggio L., Bender R., 1998, *MNRAS* 296, 119
 Thornton K., Gaudlitz M., Janka H.-Th., Steinmetz M., 1998, *ApJ* 500, 95
 Timmes F.X., Woosley S.E., Weaver T.A., 1995, *ApJS* 98, 617
 Tinsley B.M., 1980, *Fund. of Cosmic Phys.* 5, 287
 White D., 2000, *MNRAS* 312, 663
 Yepes G., Elizondo D., Ascasibar Y., 1998, *Ap&SS* 263, 31